The Development of Full Body Geometrical Data for Finite Element Models: A Multi-Modality Approach

Mimics Innovation Awards

F. S. Gayzik[1,2], D. P. Moreno[1,2], J.D. Stitzel[1,2]

1. Wake Forest University School of Medicine
   Winston-Salem, NC, 27157, USA
2. Virginia Tech – Wake Forest University Center for Injury Biomechanics
   Winston-Salem, NC, 27157, USA

Abstract

We present a review of the methods used in the development of a new full body computer aided-design (CAD) representation of a male seated vehicle occupant. The model was designed to represent 50th percentile male (M50), and is intended for subsequent use in numerical methods such as Finite Element Analysis (FEA). The purpose of this paper is twofold. First we review the methods used in each phase of model development, from subject recruitment, to imaging, to segmentation, and creation of the full body model. The second is to review key attributes of the full body CAD geometry. A healthy male subject, aged 26 years was used as the framework of the model. This individual met selection criteria after extensive pre-screening and was enrolled in the study. His height, weight, and BMI were 174.9 cm, 78.6 ± 0.77 kg, and 25.7 respectively. He showed an average deviation of 3% from 15 external anthropomorphic measurements used as selection criteria. The subject underwent a protocol consisting of both supine and upright Magnetic Resonance Imaging (MRI), as well as Computed Tomography (CT). Comprehensive external anthropometry measurements were also taken during study enrollment. The resulting images were used synergistically, along with supplemental data sources, to develop the CAD model. Segmentation revealed that nearly all internal structures agreed well with published literature in terms of morphology, location, and volume. Throughout model development, efforts were made to ensure that the model agreed reasonably well with published literature on general dimensions of anatomical features, and to that extent the current work presents a review of morphology of the average human body. The volumetric composition of the model is as follows; 9.1 % bony anatomy, 13.0 % organ, 21.7 % muscle, and finally 55.3 % of interstitial space representing skin, fascia, subcutaneous, visceral fat, and anatomical features that were not included in the M50 model. Vasculature, ligamentous, and tendinous structures were also included in the model development and account for less than 1% of the total model volume. The final CAD model consists of over 410 individual components. The structures that compose the model have been shown to be of importance in the biomechanics of traumatic injuries. The methods presented in this paper can be employed in subsequent human body model development efforts relative to injury prediction, anatomical instruction, ergonomics studies, and other applications in biomechanics.

Keywords: CAD, crash, injury, model, anatomy, geometry, finite element

Contents

Introduction

The use of computational human body models continues to grow in the study of injury biomechanics. [1] These models extend tools investigators have to study the mechanisms of traumatic injury. Models are also a cost-effective means of evaluating safety system designs in vehicular and military environments. Developers have relied on a variety of sources to describe the underlying human anatomy. External anthropometry has been studied for the development of human surrogates, both physical or virtual. [2-5] More recently, datasets for model development are commonly based on modern medical imaging techniques, as they contain highly accurate three-dimensional representations of the human anatomy.

There are a number of datasets in the published literature that are frequently used in the development of FEA models. Perhaps the most well-known of these datasets is the Visible Human Male (VHM). [6] While it is a landmark dataset, there are some drawbacks to using VHM in the development of average-sized full body models (FBMs). The subject was quite large, (90 kg, 180 cm) which would require CAD data derived from this set to be scaled downward to the population of interest. VHM data is also derived from scans of a formalin-purfused cadaver. While the use of a fixative was necessary to prevent deterioration during transport and scanning, this altered the tissue from its native state. Finally, VHM images were collected solely in the supine position. Since occupant models are designed in the upright seated position, this provides an extra challenge for model developers in translating the data. Nonetheless, the VHM dataset is extremely valuable and has been used in countless ways, including the development of a number of well-known FEA models. [7-9]

Recent full body models demonstrate that imaging techniques are not the only method for development. The full body FEA model resulting from the HUMOS project was generated from a male cadaver frozen and sectioned in the driving position. [10] The cadaver was serially sectioned in 5 mm-thick slices acquired with a 2.5 mm gap between each slice. The cadaver used in this study approximated the 50th percentile male, with stature and weight of 173 cm and 80 kg respectively. While the data was collected in the seated position, medical images of this individual were not acquired prior to sectioning, complicating the reconstruction task. Yet another set of data commonly used by the modeling community was generated by ViewPoint Datalabs / Digimation, (*St. Rose, LA, USA*). In the case of the bones, these models were digitally recorded from physical specimens. This dataset also employed VHM and has been used in past modeling efforts. [11]

In the present work, we present a novel approach to CAD model development based on a single living subject, scanned in multiple modalities and postures. Given the amount of data that is required for model reconstruction, it is clear that there is not one single imaging modality that will provide all the necessary data to develop FBMs. Instead, we describe protocols for a multi-modality approach that employ imaging techniques such as MRI and CT, as well as methods for external anthropometry data collection. We also aimed to improve upon previous model development efforts by acquiring and using scans wherein the participant is seated upright, in the correct orientation with gravity. In validating our findings, it was noted that data on the morphology of many internal organs (volume, diameters, etc.) is available but is scattered across the open literature.

Crash Induced Injuries

The data presented in this paper are intended for use the in the development of numerical models for the enhancement of safety systems. This data is directed predominantly at preventing injuries and fatalities in high-risk environments such as motor vehicle crashes. Crashes and their associated injuries remain a major public health problem worldwide. In 2008 alone there were 5.8 million police-reported crashes in the United States, resulting in 2.3 million injuries and 37,000 fatalities. [12] In light of this motivation, the model development process was guided by a finite number of specific injuries that are commonly-encountered in vehicular crashes. For the purposes of this work, we refer to such injuries as crash-induced injuries, or CIIs.

Table 1 provides an overview of targeted CIIs by body region and the associated anatomy required to model such injuries. These CIIs are specifically targeted so that the resulting CAD, and models developed from it, will have the capacity to predict the occurrence of these injuries, or at least the risk thereof. This list is not exhaustive.

Objective

The objectives of this work are twofold. The first is to present the methods used in the development of a full body CAD model that represents the average male vehicle occupant. We provide detailed methods in the recruitment, image acquisition, and scanning protocols that form the basis of the model development. We also review the methods used in segmentation and CAD development. The second objective is to present information on the resulting CAD data including the physical dimensions (volumes, surface areas, etc.) of the components of the model.

Table 1. Crash induced injuries by body region, selected associated anatomy, and references on material studies, injury values, or validation data.

Region	CII	Associated Anatomy
Head	Skull and facial fracture	All bones of skull
	Cerebral contusion	Cerebrum and gray matter
	Diffuse axonal injury	Cerebrum and white matter
	Acute subdural hematoma	Dura and arachnoid layers
Neck	Vertebral fracture	Cervical vertebrae, disks, and ligaments
	Vertebral dislocation	Cervical vertebrae, disks, and ligaments
	Whiplash	Cervical vertebrae, facet joint, to be determined
	Cord injury	Spinal cord (cervical segments)
Thorax and Upper Extremity	Rib fracture	Ribs, cortical bone differentiated
	Sternum fracture	Sternum, cortical bone differentiated
	Lung contusion	Lungs
	Aortic injury (tear, sub-failure)	Heart, aorta, regional vessels, tethers
	Long bone fracture	Clavicle, ulna, radius, humerus, cortical bone differentiated
Abdomen	Liver injury (contusion, laceration)	Liver, connective tethers
	Spleen (contusion, laceration)	Spleen, connective tethers
	Kidney (contusion, laceration)	Kidney, connective tethers
	Large vascular injury (tear, sub-failure)	Aorta, vena cava
	Tethering vasculature injury (tear)	Portal vein, superior mesenteric art. & v., inferior mesenteric art. & v. (portions), renal art. & v., splenic art. & v.
	Digestive tract (hollow organ) injury	Stomach, duodenum, proximal jejunum, distal ileum, colon
Pelvis and Lower Extremity	Rami, symphysis, sacroiliac fracture / failure	Bones of pelvis, sacrum
	Hip fracture	Acetabulum, articular cartilage
	Femur fracture	Femur, cortical bone differentiated
	Knee injuries	Major ligaments, meniscus, articular cartilage
	Hindfoot injuries	Talus, calcaneus, cortical bone differentiated, ligaments

Methods

Subject Recruitment

Subject recruitment and selection is reviewed here, but further details can be found in a previous work [13] The subject selection and imaging protocol was approved by the Wake Forest University School of Medicine Institutional Review Board (IRB, #5705). A targeted weight and height requirement was used to narrow the applicant pool. We sought a single participant who measured 175 cm and weighed 77 kg and met numerous other criteria described below. These targets were selected from pervious anthropometric studies as the average height and weight of an American male. [3] In addition, these values were used in the design of the Hybrid III male Anthropomorphic Test Device (ATD, or crash test dummy). [14] A tolerance of ± 2.5 cm on height and 5% on weight was permitted. A more focused review of applicants followed for the preliminary applicants. Exclusion criteria included claustrophobia, physical or orthopedic impediments, diagnosis of osteopenia, prior surgery, abnormal gross anatomy, and MRI risk factors. Fifteen anthropometric measurements were taken in both seated and standing positions. [2, 13] The selected subject would have to measure within on average 5% of a target value. Target values were taken from the 50% percentile male value found in a previous anthropometric study. [2] A single individual meeting all criteria was selected for the study (M50).

Image Data Collection

The individual underwent the entire imaging protocol described herein. [13] MRI image data with the participant in the supine position was collected on a 1.5 Tesla TwinSpeed MRI scanner (GE, Milwaukee, WI). A three dimensional Fast Spoiled Gradient Recalled pulse sequence used was used, wherein the TE and TR were selected such that the fat and water signals were out of phase (Figure 1A). This resulted in a darkened outline around viscera and muscles that aided segmentation of these structures. Slabs of image data were collected from head to foot. Breath-held scans were acquired in the chest and abdomen so acquisition time for these was short (appox. 30 sec.). All other scans were non-breath held.

Images were predominantly acquired in the transverse plane, although coronal images of selected anatomy were acquired in head and abdomen. A total of 43 image stacks were collected over three scanning sessions.

The upright MRI protocol utilized a 0.6 T Fonar Upright MRI (Fonar Inc., Melville, NY). Three dimensional gradient echo pulse sequences similar to those developed for the close-bore MRI scanner are used so that the resulting images are acquired with the fat and water signal out of phase (Figure 1B). Images were acquired in both the seated (head, neck, thorax, abdomen, flexed knee) and standing (shoulder, thorax, abdomen, load bearing knee) positions. The seat back angle was set to 23^{o} for the seated scans. Images are acquired using Sympulse v. 7.0 software from the scanner's manufacturer. A total of 17 image stacks were collected during a single session.

Computed tomography (CT) scans are acquired from the study subjects using a GE LightSpeed, 16-slice scanner on a Linux platform. Images were acquired in helical mode, with the subject in the supine and an approximately seated position. Scanning parameters were set to allow for the lowest practical dose. The approximately seated position was accomplished in two scans to accommodate the posture within

the restrictive bore size of 72 cm. These scans were accomplished by essentially rotating the seated position so that head / torso, and lower extremity scans could be acquired that replicated the seated position as closely as possible. [13] Specialized inserts were developed that enabled the posture of the seated scan to be maintained during these scans. Slice thickness of images used in segmentation efforts were on the order of 1 mm (Figure 1C).

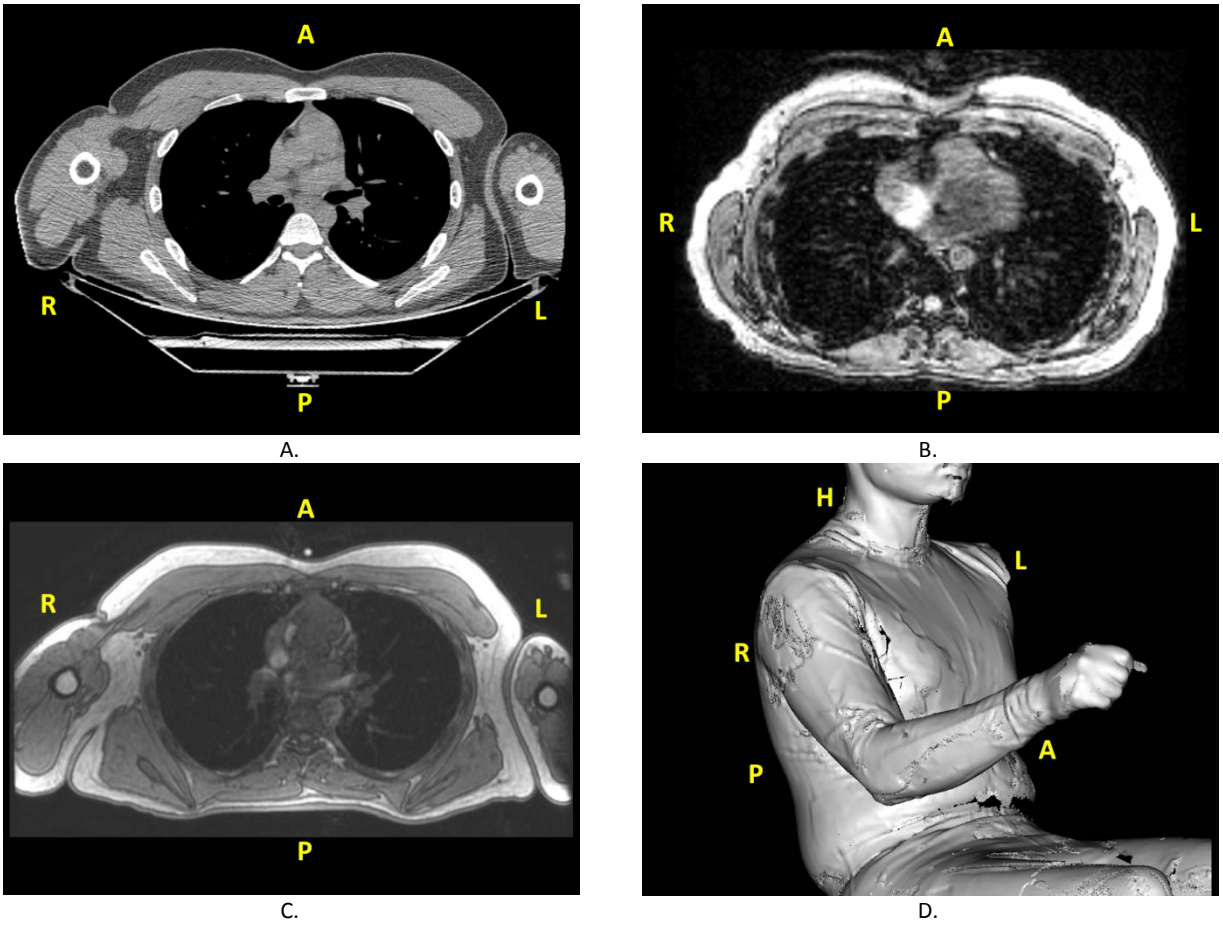

Figure 1. Overview of data collected for full body CAD development, showing examples of thorax data. A. Conventional MRI, supine, arms at sides B. Upright MRI, C. CT, supine, arms at sides, D. External body laser scan in seat buck (raw point data).

External Anthropometry

Model construction relied on extensive external anthropometry data collected from the participant. Data were collected with a 7-axis 3D digitizer. We collected data from the subject in the seated position. A seat buck was designed to acquire landmark data and un-deformed external body contours. Seat buck parameters such as wheel to ball of foot distance, and steering wheel height, were adjusted to meet seating accommodation models from previous studies. [15] Seat back and pan angles were 23^{o} from vertical and 14.5^{o} from horizontal respectively [16].

Fifty-six landmark locations (22 left, 22 right, 12 along the mid-sagittal plane) were identified through palpation. [17] These landmarks captured the posture of the subject in each body region. Landmarks were digitized using Studio software (v. 11, Geomagic, Research Triangle Park, NC).

A laser attachment was used to record the complete body shape of the M50 subject in the seat buck (Figure 1D). The dominant side of the subject's body was scanned to reduce scan time. Portions of the left side were also scanned to validate symmetry of the model (Figure 2).

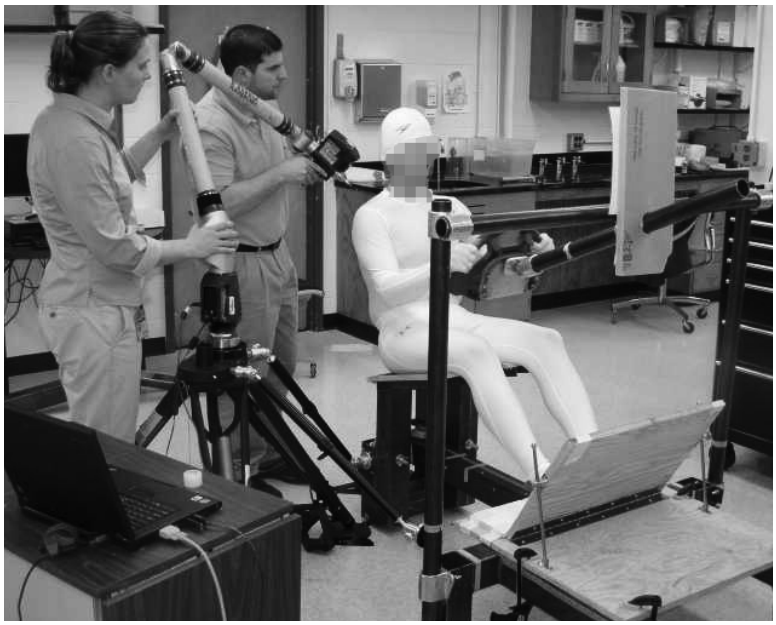

Figure 2. Custom seat buck external anthropometry data acquisition of the M50 subject. The rear right back panel has been removed.

Preparation of Image and External Anthropometry Data

All images were reviewed by a faculty radiologist at Wake Forest University Baptist Medical Center prior to use. In many cases it was advantageous to merge and align two or more adjacent image slabs that depicted into a single continuous slab. This procedure facilitated subsequent segmentation as well as assembly efforts. Adjacent image slabs were combined using Amira image analysis software (v. 5.2, Visage Imaging, Andover, MA). The initial alignment relied on a user to collocate two adjacent slabs in the same image space. Images were roughly aligned along the axis normal to the transverse slices. The result of this process was a single set of images representing the sum of two or more slabs.

Merged and aligned image sets were used in segmentation for all body regions. These included supine abdominal MRI, lower extremity MRI, and upper extremity MRI. CT scans were also merged to create full body image slabs. Of particular utility was a combination of slabs from the upright MRI scans, with the participant in the seated position. In this set, six slabs of transverse images depicting the neck, thorax, abdomen, and pelvis were combined and used as a framework for model development in the seated posture (Figure 3).

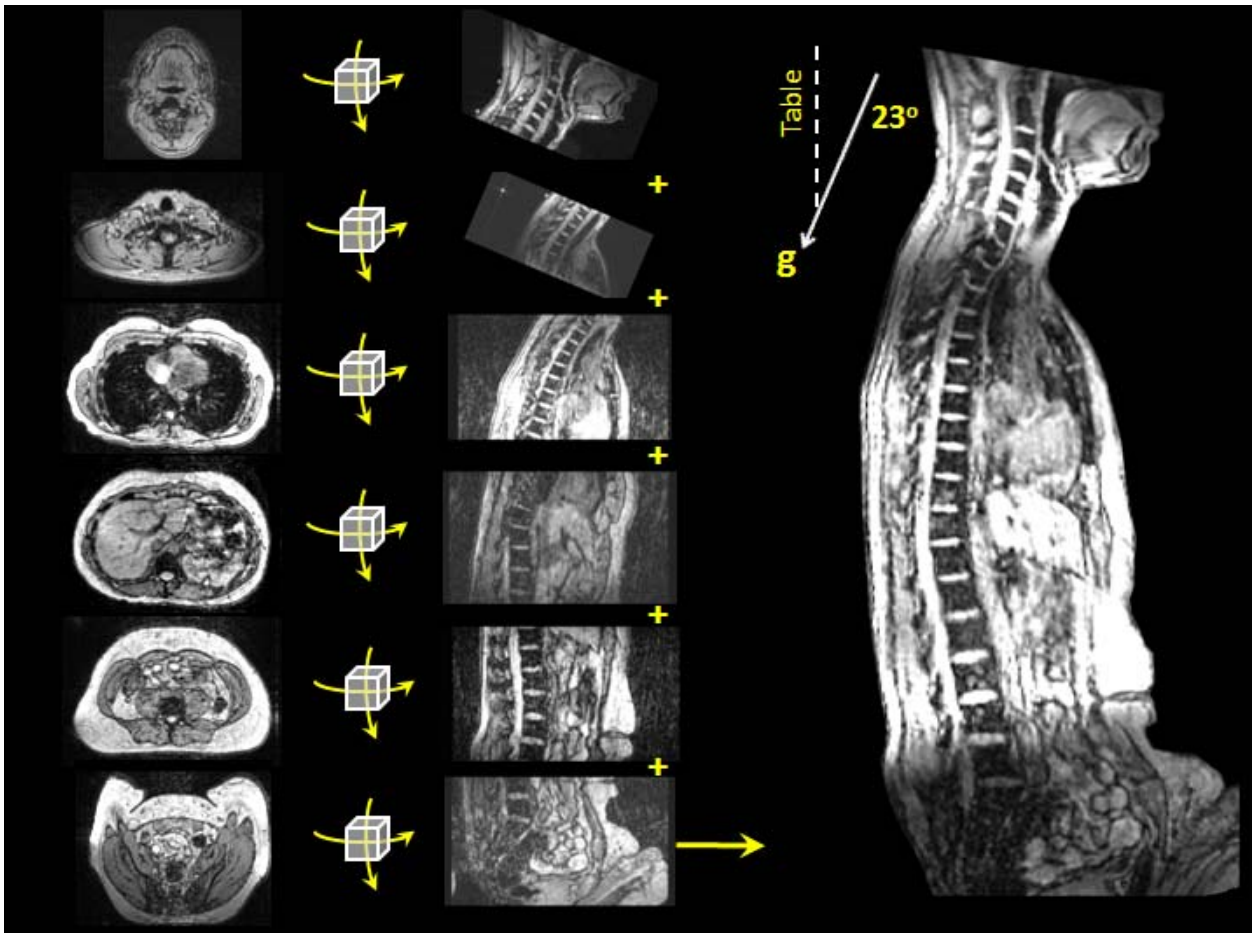

Figure 3. Schematic process of merging and aligning image sets. Left column, transverse Upright MRI slices. Middle column, slab is rotated for sagittal viewing. Scans were combined into a single slab from the occipital condyle to the sacrum. Images are relative to upright MRI seat back, which was rotated 23° counterclockwise to match seat buck. The direction of gravity is indicated.

Raw landmark data and surface contours from the external anthropometry scans were reduced for use in model development. A symmetry plane was calculated via a least squares plane fit using landmarks located along the sagittal midplane. These included vertebral column landmarks, and the top of the head, and the pubic symphysis. Right side landmarks were mirrored to ensure that the final landmark set was symmetric about the sagittal midplane. External body contours (Figure 1D) were converted to polygon data, and mirrored about the sagittal midplane.

Model Development Approach

A schematic of the overall model development process is shown in Figure 4. Image segmentation was the beginning of the process. In the next phase, three dimensional polygon data extracted from image segmentations were conditioned to remove artifacts, and to verify against literature data. The assembly phase involved repositioning segmented and conditioned models to align with scans taken in an upright and seated posture. Finally, mathematical CAD surfaces composed of Non-Uniform Rational B-Splines (NURBS) were overlaid onto the polygon data. We returned to the polygon data as necessary to remove overlapping or penetrating structures noted in the assembly.

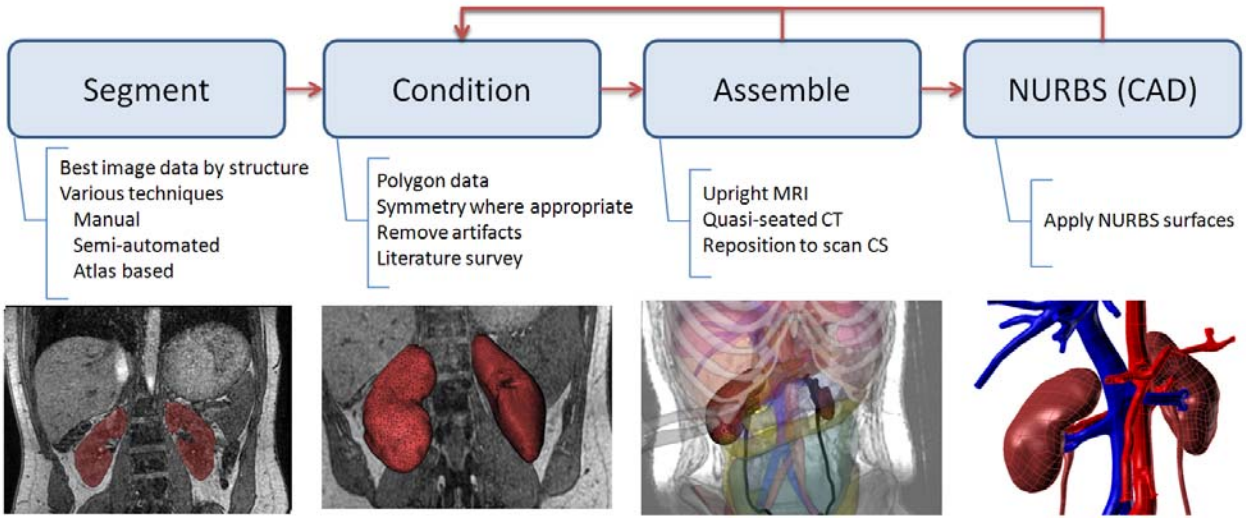

Figure 4. Model development phases for full body CAD.

Segmentation, conditioning, and assembly by tissue type

Mimics software was used exclusively for segmentation (v. 13.0, Materialise, Leuven, Belgium). Remaining steps were completed using a variety of supporting software packages.

Bone

All bones of the body were individually segmented from the CT data. Applicable bone segmentation and image processing methods were tested to facilitate segmentation. [18, 19] Selected automated and semi-automated bone segmentation methods were conducted on the M50 tibia for as a trial. Due to a number of limitations of the automated algorithms; often these are developed for specific bones, or only limited information on implementation is available in the published literature, we applied a semi-automated procedure to the complete the bony segmentation.

Bone segmentation began by selecting pixels exceeding 226 HU. Bones with small articular spaces (such as cervical and thoracic vertebra) were manually separated. Standard segmentation operations such as region growing, morphological operations, and multi-slice linear interpolation were used. For the majority of bones only the periosteal surface was of interest to the modeling effort. These bones were exported from the segmentation software as a 3D polygon shell.

The polygon surfaces were conditioned to remove artifacts and any structural abnormalities that were found in the resulting segmentations. The segmentation and conditioning process for a sample bone is shown in Figure 5. For many of the bones along the axial skeleton, symmetry was enforced. Following the mirroring process, deviations from the original segmented polygon were conducted to verify that significant structural changes had not been introduced in this process (Figure 5C).

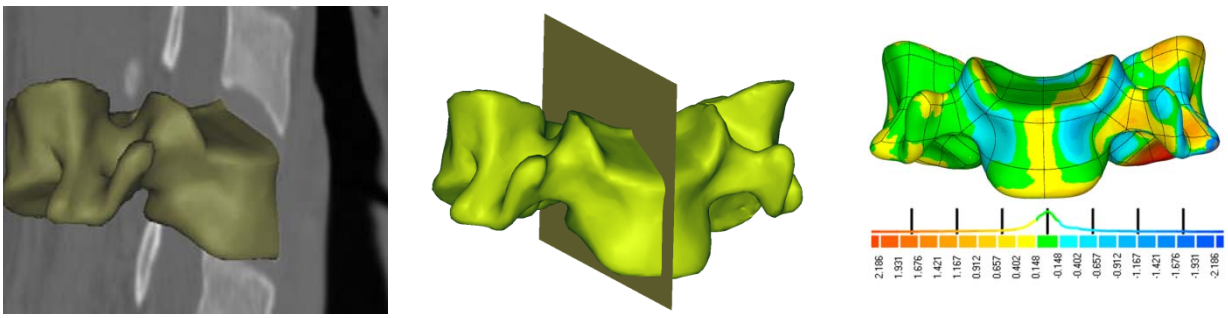

A. B. C.

Figure 5. Bone segmentation and conditioning process. A. Bone (C5) from segmentation, B. C5, with symmetry plane fit, C. C5, mirrored, showing deviations from original segmentation (Units: mm).

For a number of bones, the CII modeling requirement called for two concentric bone surfaces. One represented the perosteal surface of the bone, and a second, within the first, represented the endosteal layer of the cortical bone. Periosteal bone surfaces were determined using the method above. For endosteal cortical surfaces, thickness samples within the image were taken at diaphyseal and epiphyseal regions (in the case of long bones), or in various sub structures of the bone (such as the pubis, ilium and ischium of the pelvis). Thicknesses were estimated using 50% of the full width of a gray-scale profile line perpendicular to the bone. [18] The resulting exterior and interior layers were then manually refined against the original CT images.

Previous CT research has shown that segmentation accuracy begins to break down when the thickness of a structure of interest falls below 1.5 times the full width half max (FWHM) of the point spread function (PSF) of the scanner used. [20, 21] Based on the field of view used in our scans, and data from previous investigations using a similar scanner, [22] we set the limit threshold for thickness segmentation at 2.75 mm. Thus, when the segmented cortical thickness fell below this value, we deferred to literature studies for the thickness (Figure 6). The midshaft portion thickness values from the image sets were validated against literature sources.

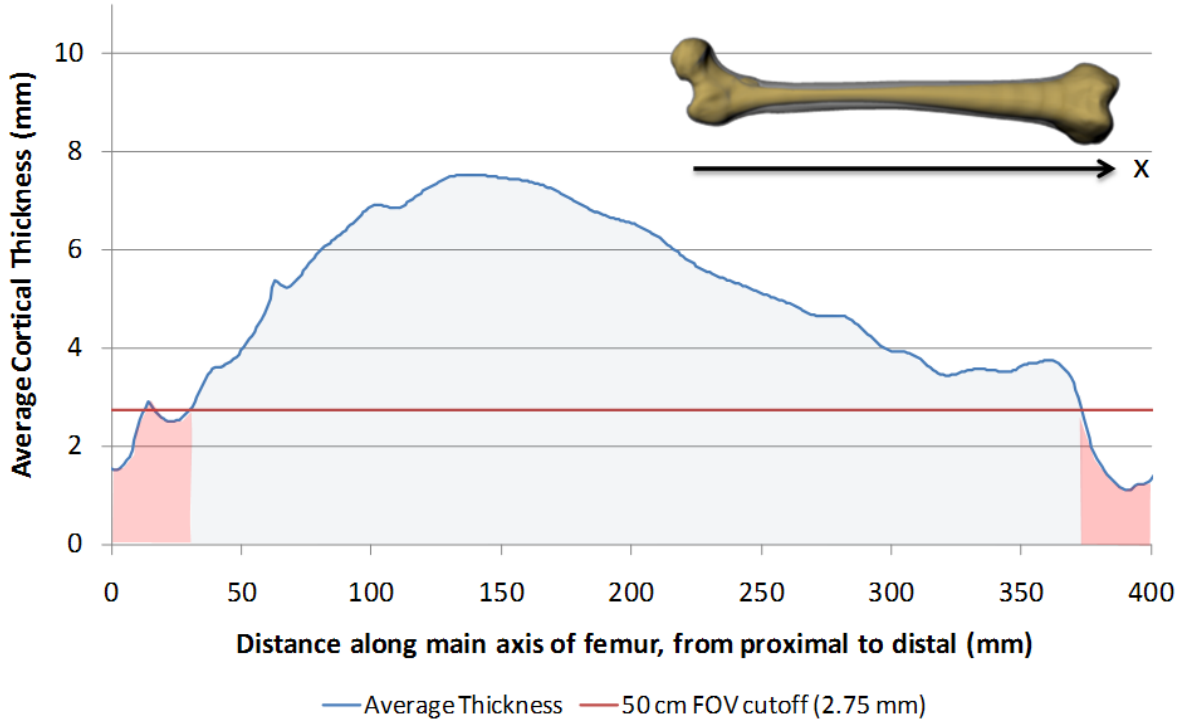

Figure 6. Femur thickness calculation along midshaft. Cutoff value based 50 cm field of view is shown (2.75 mm). Shaded green indicates regions where cortical thickness was used from scan, red where literature values were used.

Bones were assembled by relocating each from the CS of the CT image set from which they were segmented to the model CS.

Organ

Like bone, organ segmentation was accomplished in Mimics. Organ segmentation also followed the needs outlined by the CIIs found in Table 1. Segmentation was done using supine MRI data from the subject. The majority of organ segmentation was conducted manually using standard techniques to facilitate the process, including dynamic region growing, multi-slice editing, and morphological operations.

After initial segmentation in supine MRI, 3D polygon models were transformed into the space of the upright MRI data in Mimics (Figure 3). Since that data was taken in the seated position, it was the truest representation of the morphology and location of the organs in the seated posture. Within the head, this data was used to match the distribution of Cerebrospinal Fluid (CSF) between the inner table of the skull and the cortex of the brain (Figure 7).

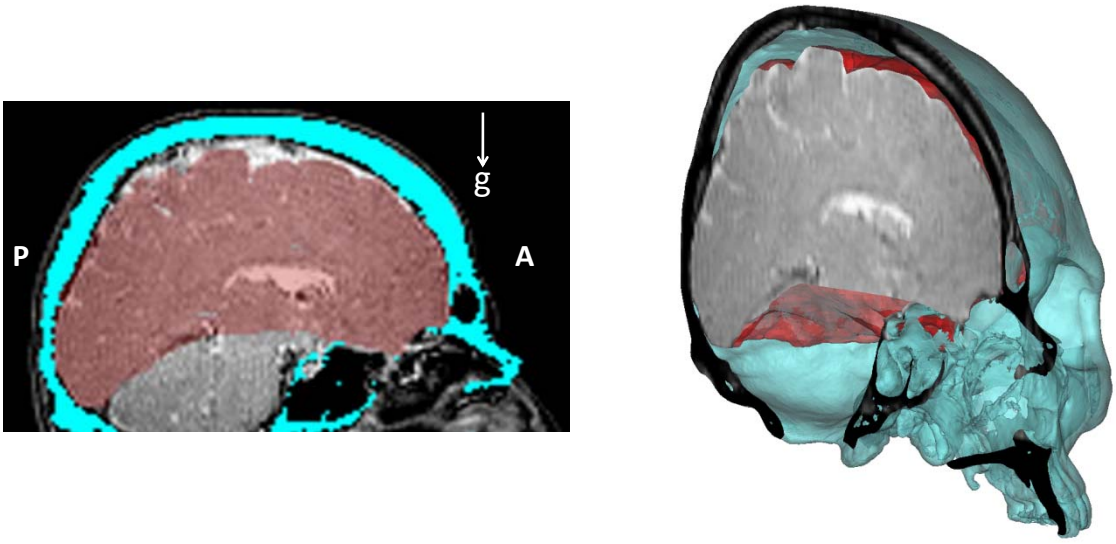

A. B.

Figure 7. A. Segmentation of cerebrum and skull in upright MRI image coordinate system, showing cerebrum mask (red), skull mask (cyan) and CSF (bright). Direction of gravity noted. B. Oblique view of A, with rendering of 3D model showing CSF cavity.

The mediastinum, and abdominal cavity (peritoneum, retroperitoneum, and perineum) were segmented in the upright scan (Figure 8). In many cases, the resolution of the upright scan did not provide as accurate a segmentation of the structures of interest, so detailed segmentations from the supine scan were imported into the upright scan CS and positioned to the location of the organ in the upright scan.

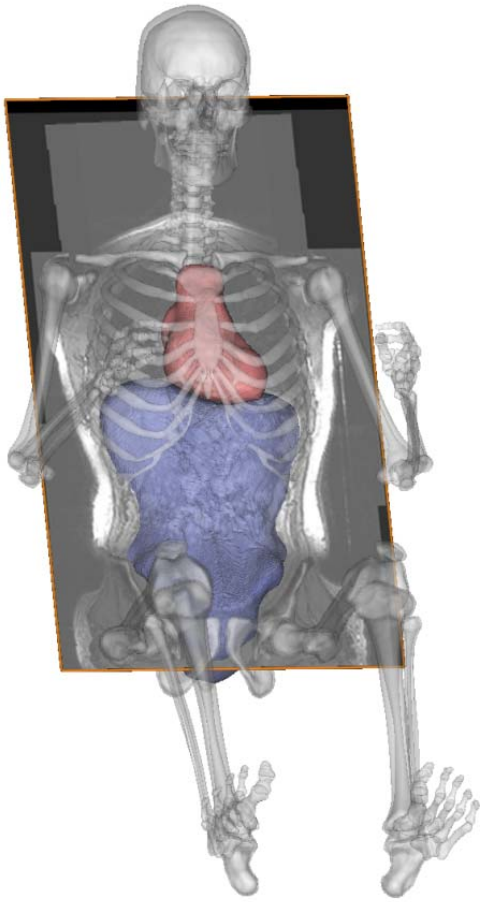

Figure 8. Compartmentalization approach showing skeleton and major cavities used in CAD assembly (mediastinum, red, abdominal, blue). Objects are overlaid on the coronal plane of the image stack.

Vessels

Where possible, vasculature was segmented from the MRI and CT scans of M50. However, scans for this work were not contrast-enhanced. Foreseeing the need for such data, a contrast-enhanced CT scan was obtained from the image database at Wake Forest University Baptist Medical Center. The scan depicts an approximately 50th percentile male (21 years, weight, 79 kg, height, 185 cm) who had not suffered injury to the thorax or abdomen.

A centerline approach was developed to implement tethering vessels within the thorax and abdomen. The approach is shown in Figure 9. Following segmentation, a center line feature within Mimics software was used to reduce the vessel to only its essential trajectory.

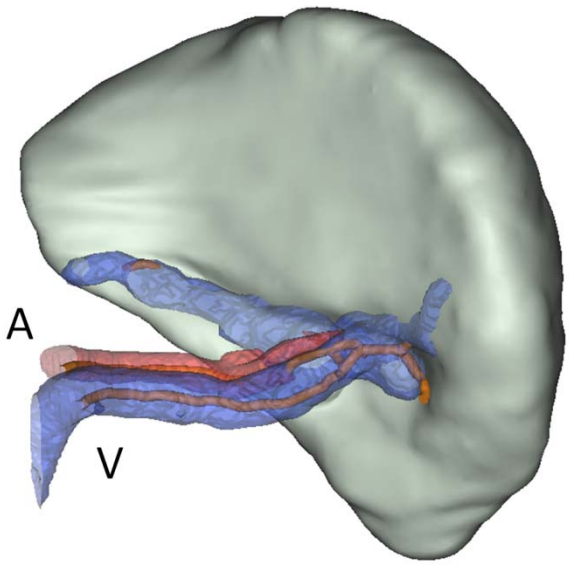

Figure 9. Center line approach to developing vasculature in M50. Segmented vasculature (splenic artery and vein) is transparent showing underlying reduced centerline.

Muscle

Muscles were segmented for the model development effort as were germane to modeling CIIs (Table 1). In each body region, muscles were directly segmented from the supine MRI image data using techniques described above (dynamic region growing, multi-slice editing, and morphological operations). The selection of the pulse sequence, was especially well suited for segmenting large muscle groups as a clear outline was visible in most cases (Figure 10).

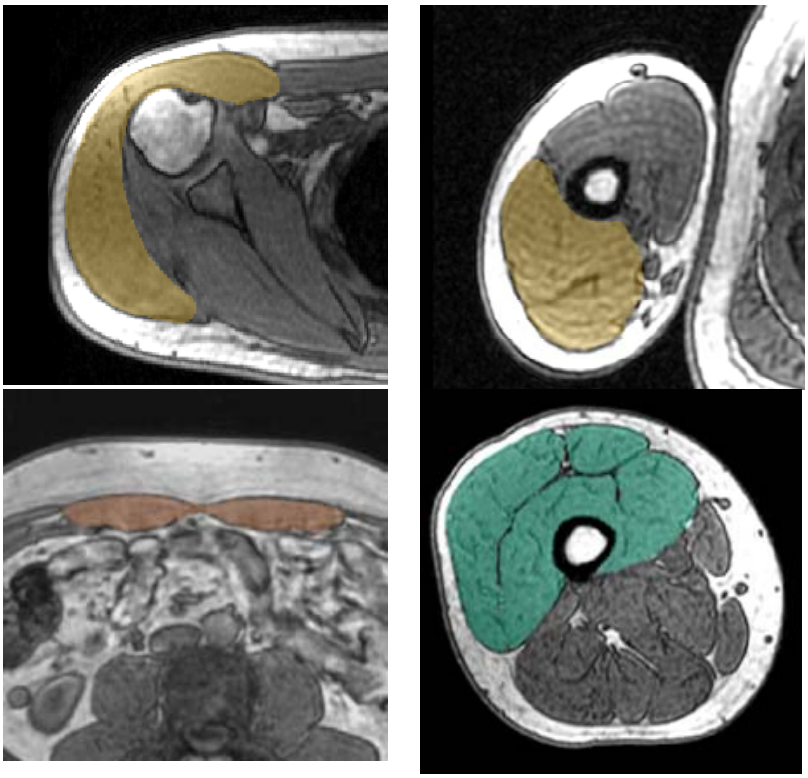

Figure 10. Examples of muscle segmentation, clockwise from top left; deltoid, triceps brachii, rectus abdominis, and quadriceps femoris.

With regards to muscle segmentation, the regional neck segmentation effort is noteworthy. Fifty-two muscles of the neck, were explicitly segmented This included 26 on each side, with the only grouped muscles being sternothyroid and thyrohyoid. [23] In some cases, neck muscles segmentation was not possible using the 1.5 T scans of the neck. In these cases, we referred to high-resolution digitized photographs of anatomical cross sections of the Visible Human Project. [6]

Cartilage, Fibrocartilage, Ligament and Tendon

A limited amount of cartilage, fibrocartilage, ligament, and tendon anatomy were included in the model. These were segmented manually using the methods described above. These specifically include the costal cartilage, articular cartilage of the knee (femoral, tibial, and patellar), ligaments of the knee, the menisci, and the calcaneus tendon.

External Skin Surface

An outer skin surface was also developed for M50. The skin surface was largely developed from the external anthropometry portion of the study. The data underwent similar conditioning as segmented portions from the images

CAD Development

The final stage of model development was the CAD phase. Here, the conditioned polygon data was converted to a mathematically defined NURBS patchwork. The first process (data conditioning) was

described in the previous section. Border continuity is enforced such that the patchwork is G1 continuous.

Results

The selected individual was a 26 year old male. His height, weight, and BMI were 174.9 cm, 78.6 ± 0.77 kg, and 25.7 respectively. The subject passed all exclusion criteria, had a clean medical history, and was generally in excellent health. The subject was been deemed to have typical anatomy, exhibiting no major anatomical abnormality or major pathologic condition by our collaborating radiologists. Given the amount of scans that were required, the final image parameters used were the results of a balance between acquisition time and signal-to-noise ratio. Results are presented by tissue type.

The volumetric composition of the model is as follows; 9.1 % bony anatomy, 13.0 % organ, 21.7 % muscle, and finally 55.3 % of interstitial space representing skin, fascia, subcutaneous, visceral fat, and anatomical features that were not included in the model. Vasculature, ligamentous, and tendinous structures were also included in the model development and account for less than 1% of the total model volume.

CAD Summary

The final model comprises the necessary elements for biomechanical modeling efforts of the mid-sized male in the seated position. There are 410 individual components of the full body; 179 bones, 46 organs and components thereof, 96 muscles, 37 vessels and 46 ligaments, tendons and other cartilaginous structures. The model is sagittally symmetric. The volumetric composition of the model is as follows; 9.1 % bony anatomy, 13.0 % organ, 21.7 % muscle and finally 55.3 % of interstitial space representing skin, fascia, subcutaneous, visceral fat, and anatomical features that were not included in the model. Vasculature, ligamentous, and tendinous structures were also included in the model development and account for less than 1% of the total model volume. The model is composed of mathematically defined, NURBS surfaces.

Skeletal system of M50

The entire skeletal system of the human body is represented in the model, a total of 179 bones. Figure 11 shows the final bony assembly along with the external anthropometry landmark data points. Significant detail is found in the geometry including; sinuses of the skull, vertebral foramina, transition locations of rib cortical surface to rib cartilage, sacral foramina, and relevant protuberances in the lower extremity for muscle attachment. Close agreement with the selected landmarks and corresponding bony locations were noted in the assembly.

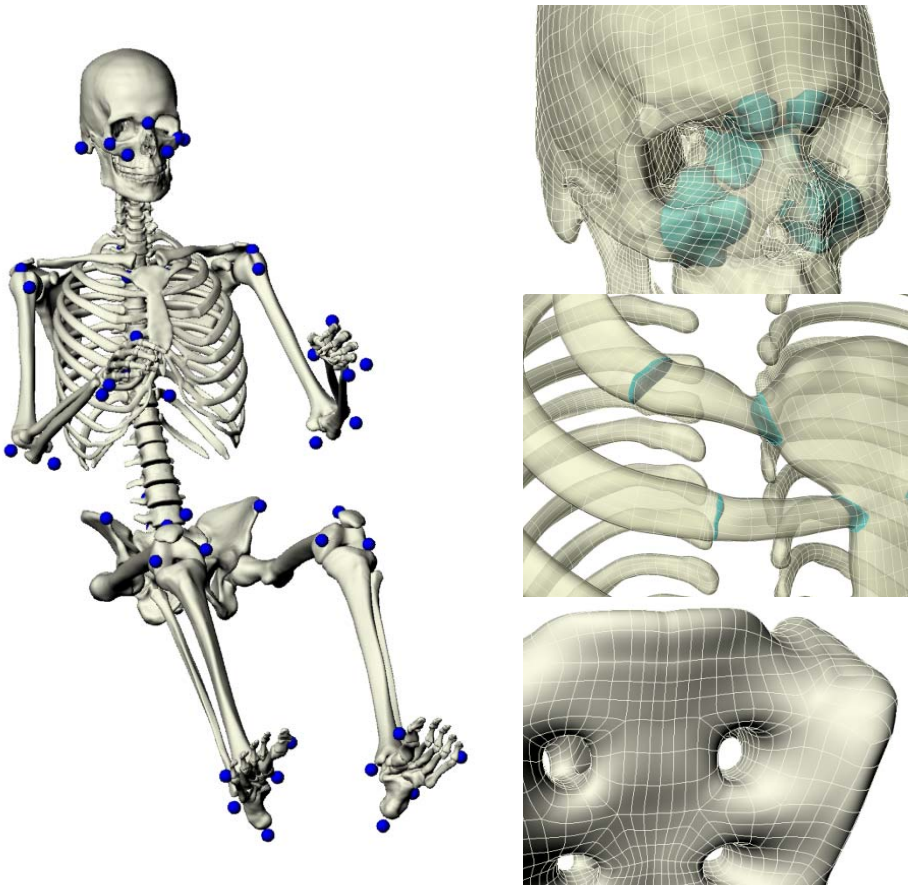

Figure 11. Final bony assembly of M50 CAD model, with external landmark data points for subject. Landmarks are represented by 1 cm spheres for visualization. Detail images from top to bottom show sinus cavities, costal cartilage with bone transition surfaces, and sacrum.

For a number of bones, both periosteal and endosteal surfaces were required. Due to scan resolution limitations, some portion of the CAD data for these bones was taken from literature data. For most long bones, modifications were made at the epiphyseal ends per the methods section. These modifications are cataloged in Table 2. Midshaft values reported correspond to average thickness of the mid-third of the bone along the long axis. Figure 12 shows an example of the results of this modeling effort for the femur, with a corresponding cortical thickness map. For other bones, the entire cortical thickness fell below the threshold of 2.75 mm described in the methods section. For these bones, a constant thickness offset of the exterior surface was used to model the endosteal surface. These bones were the sternum (1.5 mm), sacrum (1.0 mm), patella, (0.6 mm), talus (0.45 mm) and calcaneus (0.45 mm). Data on the cortical thickness of the pelvis can be found in the literature, however separate CAD surfaces for this bone were not constructed. Surfaces indicating the border of the medullary cavity of the long bones of the lower extremity are also included.

Table 2. Bone CAD objects with epiphyseal modifications, showing regions below image precision threshold of 2.75 mm.

Bone	Region below threshold	Prescribed Epiphyseal Thickness (mm)	Mean midshaft thickness (mm)
Clavicle	Full shaft < 2.75 mm threshold	1.0	2.0†
Scapula	Glenoid fossa	0.6	2.68 ± 0.63
Humerus	Distal and Proximal Epiphyses	1.0	6.12 ± 0.27
Radius		1.0	4.31 ± 0.26
Ulna		1.0	4.80 ± 0.25
Femur		1.0+	6.17 ± 0.98+
Femural neck	Full structure	1.5 - 3.5	-
Tibia	Distal and Proximal Epiphyses	1.0	6.74 ± 0.73
Fibula		1.0	4.17 ± 0.07

† Prescribed, *Thickness along lateral border, + See Figure 6, Figure 12.

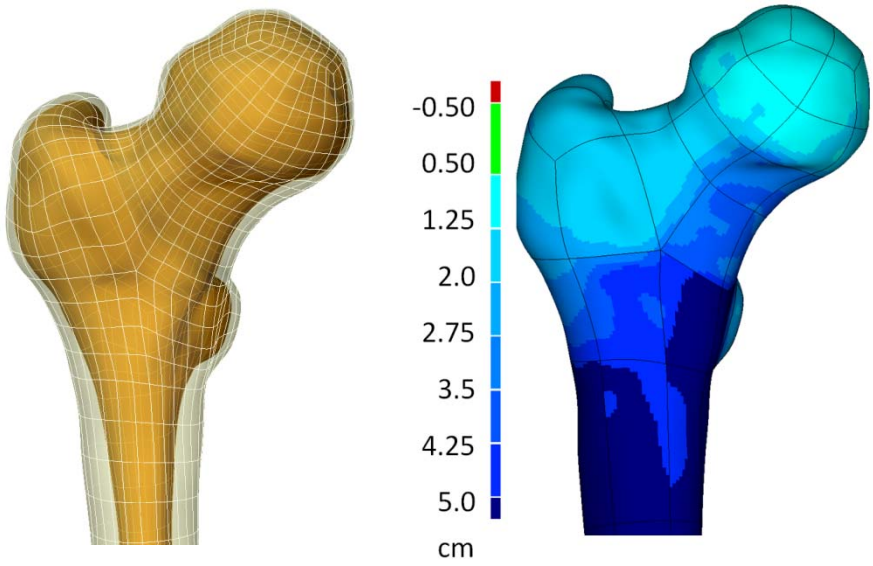

Figure 12. Example of cortical bone modeling effort at the proximal femur (left). The outer cortical layer is transparent, the inner layer in yellow. The corresponding cortical thickness map (right).

Organ systems of M50

The nervous system modeling efforts focused on the brain and spinal cord. The brain model contains the cerebrum, venous sinuses (transverse, superior), ventricles (lateral, 3rd, 4th), brainstem, basal ganglia, corpus callosum, fornix, thalamus, cerebellum, falx,and tentorium (Table 3, Figure 13). All structures in the M50 brain model were isolated from the supine MRI images, with the exception of the falx cerebri and tentorium. These were constructed in CAD as reliable segmentation of such thin structures was not possible.

Table 3. Selected brain structures from the M50 model with volumes vs. literature.

Structure	M50 Volume (cm^3)
Basal Ganglia	19.4
Cerebellum	141.8
Cerebrum	1021.1
Corpus Callosum	20.1
Ventricles (Lateral, 3rd, 4th)†	22.9
Thalamus & Brainstem†	34.5

† Volumes summed

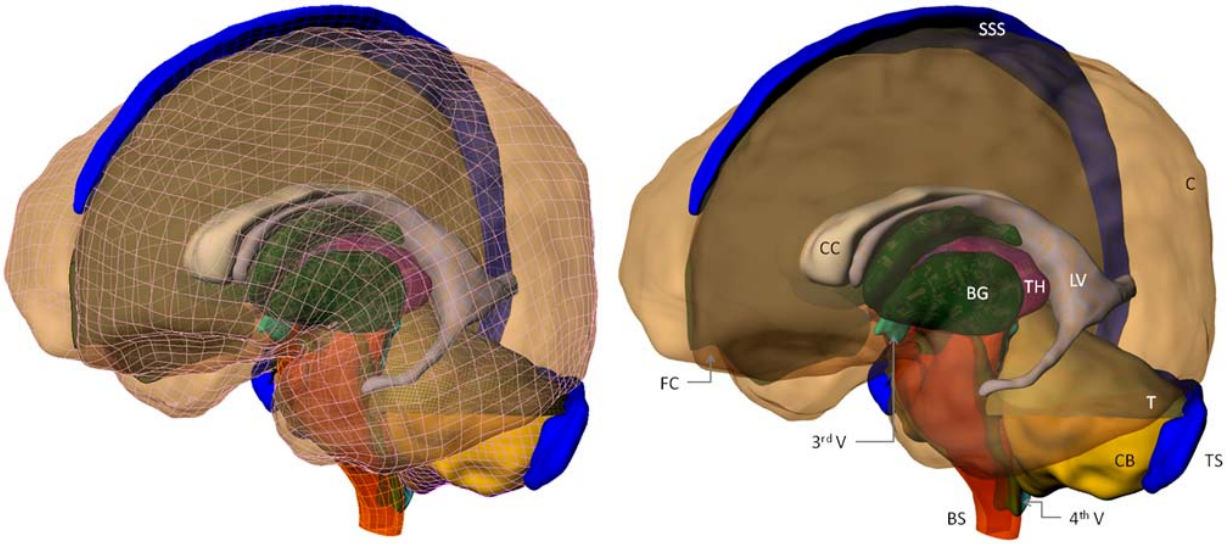

Figure 13. M50 Brain CAD model showing detailed structures. C – cerebrum (transparent), SSS – superior sagittal sinus, TS – transverse sinus, LV – lateral ventricle, 3rd V – 3rd ventricle, 4th V – 4th ventricle, BS – brainstem (transparent), BG - basal ganglia, CC - corpus callosum, TH - thalamus, CB - cerebellum, FC – falx cerebri, T – tentorium (transparent). The fornix is included but not visible.

The M50 model provides a detailed CAD reconstruction of the thoracic and abdominal viscera (Figure 14, Table 4). Regarding major organs of the respiratory system, the lungs were included in the model due to the prevalence of pulmonary contusions in vehicular crashes. Major components of the circulatory system were modeled in detail, with the heart and great vessels being the most prominent. Primary and secondary branches off of major arteries were included, so that their role as organ tethers could be modeled. Components of the digestive system were modeled, including the stomach, liver, duodenum, proximal jejunum, distal ileum, and all portions of the colon. Components of the urinary system were modeled including the kidneys, ureters and bladder. The pancreas and spleen are also represented.

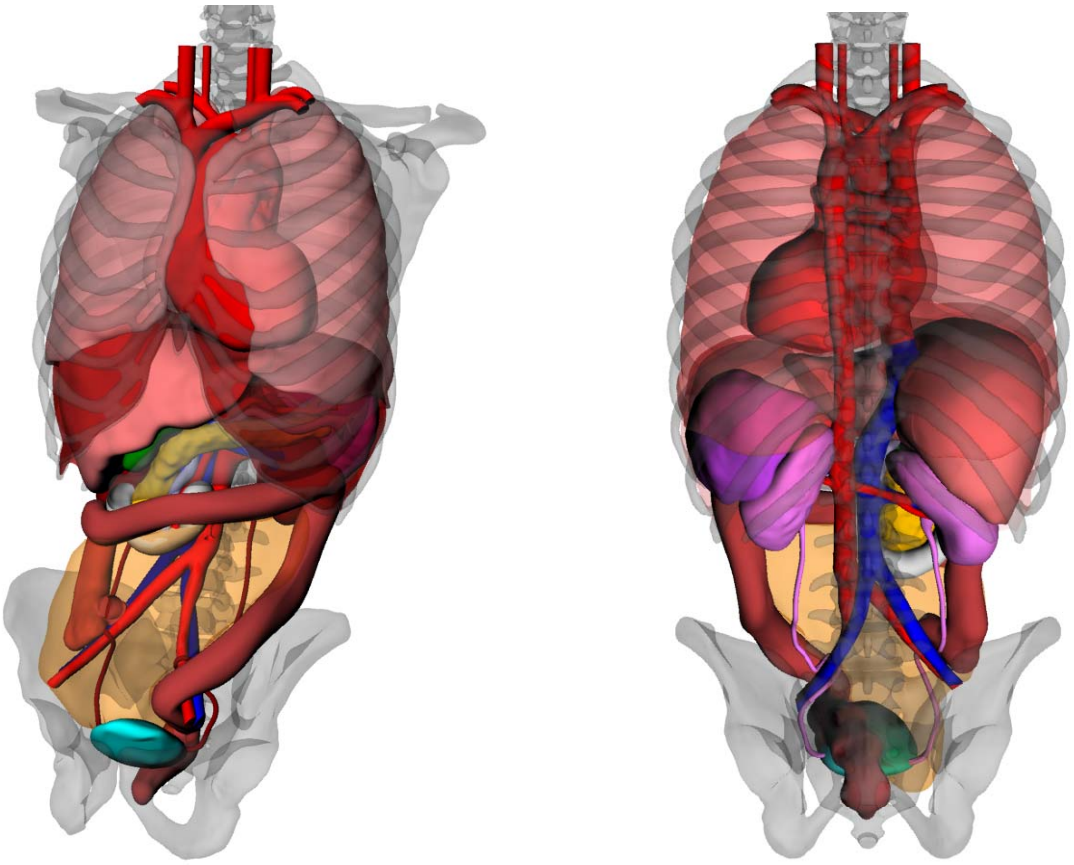

A. B.

Figure 14. Thoracic and abdominal organ contents (See Table 4 and Table 5), with axial skeleton overlay. Anterior oblique view (A) and posterior view (B).

Table 4. Thoracic and abdominal organ structures with volumes as compared to literature.

Structure	M50 value: Volume (V, cm^3) Surface area (SA, cm^2), or Diameter (D, cm)	
Heart	V	681.0
Lung (L)	V	1729
Lung (R)	V	1801
Sum L and R Lungs†	V	3530
Diaphragm	SA	1025
Stomach	V	653.3
Liver	V	1435
Gallbladder	V	15.3
Pancreas	V	77.7
Duodenum	D	2.2
Jejunum (Proximal)	D	2.1
Colon	D	2.0 – 4.0
Left Kidney	V	145.2
Right Kidney	V	146.4

Structure	M50 value: Volume (V, cm^3) Surface area (SA, cm^2), or Diameter (D, cm)	
Sum Kidneys	V	291.6
Bladder	V	99.6
Ureters	D	0.4
Spleen	V	188.7

† Volume at Functional residual capacity (FRC).

Table 5 provides vessel diameters used in this work. Most vessels exhibited more uniform vessel diameter so the diameter values in the table reflect a single measure at the midpoint of the structure.

Table 5. Typical diameter of selected vessels included in M50 model with literature range if available.

Vessel	M50 Diameter (mm)
Arteries	
Ascending aorta	28.4
Descending aorta	16.0
Pulmonary	24.0
Common carotid	6.6
Subclavian	8.4
Celiac trunk	8.5
Splenic	6.3
Hepatic	6.1
Renal	6.5
Superior mesenteric	7.3
Inferior mesenteric	3.3
Common Iliac	10.5
Veins	
Vena cava*	20*
Pulmonary	16.0
Subclavian	11.0
Internal jugular	13.0
Portal	12.8
Splenic	6.7
Superior mesenteric	10.0
Renal	9.0
Common Iliac	12.0

* Superior & Inferior

Muscular components of M50

Various major muscles are included in the M50 model (Figure 15). There are 50 muscles on each side of the sagittal midplane, with 26 muscles of the neck, and 24 muscles throughout the thorax, abdomen, and extremities. Selected components were included as needed to model the CIIs in Table 1. Muscles of the thorax, upper extremity, abdomen, and lower extremity are found in Table 6 along with volumetric validation data where available. Volumes in this table are for a single side of the body. Careful attention was given to anatomically accurate insertion and origin points on the bony skeleton.

Figure 16 provides a detailed image of the muscles of the neck. Origin and insertion points of the neck muscles are found on the skull, cervical spine, thoracic spine, rib cage, and scapula.

Figure 15. Muscular components of the M50 model (See Table 6, Figure 16).

Table 6. Muscle components of the M50 model (not including neck muscles) with literature comparison where available.

Region	Muscle	M50 Volume (cm^3)
Neck	Multiple (n=26)	419.4
Upper Ex.	Deltoid	460.5
	Biceps brachii	186.2
	Triceps brachii	460.3
Thorax	Pectoralis major	368.7
	Rhomboid major	25.6
	Trapezius (lower)†	39.6
	Latissimus dorsi	362.4
	Diaphragm‡ (cm^2)	997.3
Abdomen	Quadratus lumborum	65.6
	Transverse abdominis*	419.4
	Internal oblique*	
	External oblique*	
	Rectus abdominis	251.2
	Erector spinae††	465.2
	Iliacus	141.7
	Psoas (minor and major)*	210.1
	Levator ani	67.1
	Piriformis	42.0
	Obturator internus	57.2
Lower Ex.	Quadriceps femoris	1897.2
	Gluteus maximus	1298.6
	Gastrocnemius (medial and lateral)	412.0
	Plantaris	6.9
	Soleus (medial and lateral)	463.2

† Middle and upper portions included in neck muscle group. ‡ Surface area at FRC. * Grouped as a single component of M50. †† Portions of this muscle were included from the level of the 8^{th} rib and below.

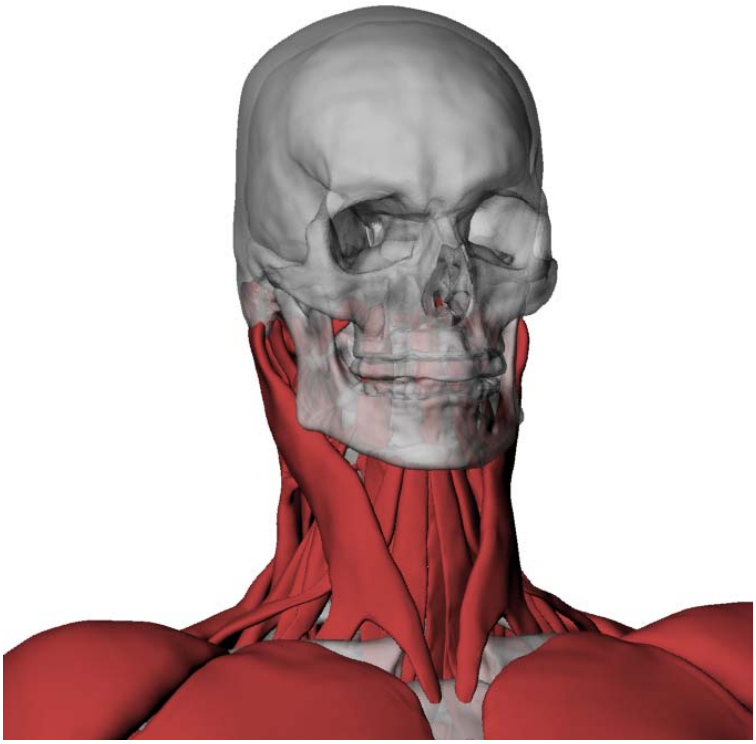

Figure 16. Oblique view showing neck musculature of M50 model.

Ligamentous, and cartilaginous components of the M50 model CAD

A limited number of ligamentous, tendinous, and cartilaginous components were included in the M50 model. As this CAD data will be used predominantly in an FEA modeling effort, many such structures would likely be included directly as beam or shell elements. Instead of replicating many of these structures, we focused only on a limited number articular cartilage structures, ligaments, and tendons that could be reliably segmented and affected the biomechanics of the region of interest. These structures were found predominantly in the knee (Figure 17) and are shown in Table 7.

Table 7. Lengths and cross sectional areas of ligaments and tendons of the M50 lower extremity.

Structure	M50 value: Max Length (L, mm), Mid-length cross sectional area (CSA, mm^2)
ACL	L: 34.9 mm
	CSA: 34.3 mm^2
PCL	L: 38.9 mm
	CSA: 49.0 mm^2
MCL	L: 90 mm
	CSA: 35.6 mm^2
LCL	L: 58 mm
	CSA: 20.4 mm^2
Patellar ligament	L: 46.0 mm
	CSA: 119.0 mm^2
Quadriceps tendon†	L: 81.9 mm
	CSA: 265 mm^2
Calcaneal tendon†	L: 247 mm
	CSA: 58.9 mm^2

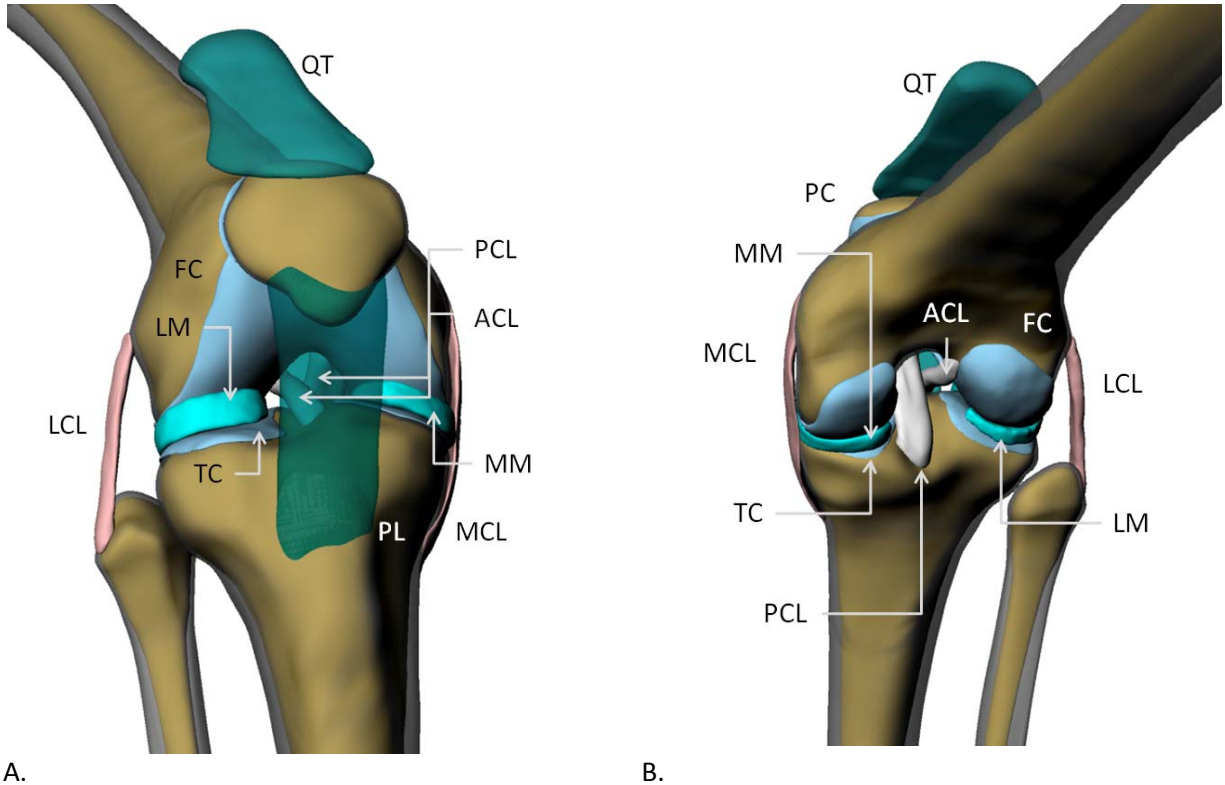

A. B.

Figure 17. Components of the M50 knee CAD. A. Oblique anterior view (PL transparent), B. Oblique posterior view. FC – femur cartilage, TC – tibial cartilage, PC – patellar cartilage, QT – quadriceps tendon, PL – patellar ligament

Skin component of the M50 model CAD

The final component of the model is a single layer representing the external skin. This component of the model is shown in Figure 18. The skin provides novel data in that undeformed contours of the lower back, buttocks, and posterior thigh were obtained through the use of the drop-away panels on the seat buck. In some regions, particularly the abdomen, comparisons with image data and external measurements on the M50 participant indicated that breathing or motion artifacts affected the accuracy of the skin layer. This was remedied by using image data to supplement the external scanning data.

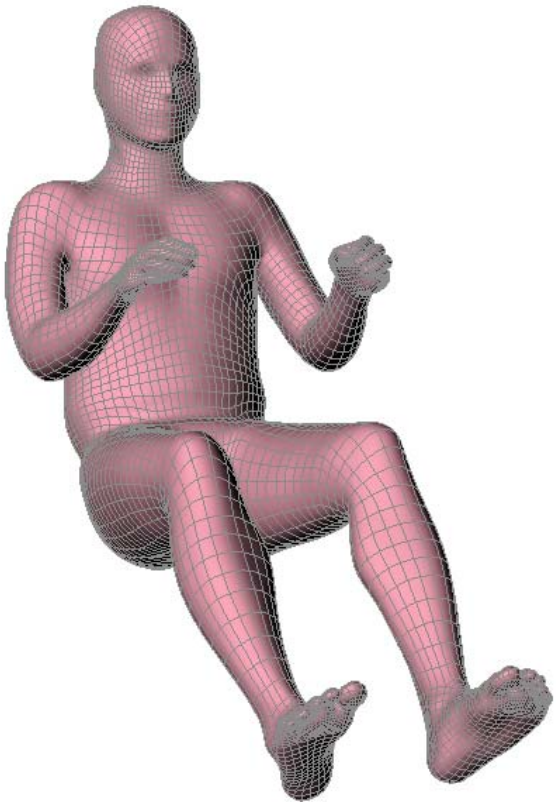

Figure 18. External skin layer of the M50 model, shown transparent over the underlying bones.

Discussion

This paper reviews the development methods employed to generate a full body CAD model of the 50th percentile male in the seated posture. We have presented our methods along the complete development of this model, from subject selection, to image acquisition, to CAD development.

We believe that there are a number of inherent advantages to the approach we have chosen for this study, beginning with subject selection. All bony data and nearly all soft tissue data in the M50 model was derived from scan of a living subject who was thoroughly screened prior to acceptance into the study. The subject met a large set of acceptance criteria ranging from his anthropometry to MRI compliance. With a height and weight of 78.6 kg and 175 cm, the subject was selected because of his close match of the 50th percentile male of the U.S. population. This is an important result since the principal use of the CAD data presented in this work will be the development of FEA models for injury prediction, and design of preventative measures in vehicle crash environments.

The dataset used in the development of the CAD model is distinct from many of the other sets of data that have been used in the development of full body models. Many of these sets contain cadaveric data, from individuals of an advanced age, or of a dramatically different size than the mid-sized male. None are in the upright position during the scanning process. While the study involved a single individual, we have made efforts, by literature comparisons, to ensure that the components of the M50 model agree with broader studies.

The each structure of CAD data is watertight with a tolerance of 0.01 mm. We have tried to develop these structures in such a way that they are amenable to FEA or CFD meshing. As they do in the human body, structures vary greatly. Depending on the scale with injury biomechanics is studies, the scale of the object under study vs. its importance is highly variable. On the contrary in developing the M50 model, we focused on developing a model that would be useful in simulating a key number of crash induced injuries (Table 1). Each of these injuries is not only prevalent, but can be modeled at the continuum level, allowing for reasonable element sizes (on the order of 2-3 mm) and run times. Thus the development of this set of CAD was done with its practical implementation in mind.

Segmentation was limited by the capabilities of discriminating thin structures or structures with low contrast with their surroundings using clinical imaging techniques. This was true with respect to cortical bone, where many structures were thinner than the minimum thickness threshold of 2.75 mm. This challenge was met by implementing CAD data in these region based on literature data on the cortical thickness of these specific bones (Table 2, Figure 6).

The potential economic and social impact of advanced computer models for safety system design is significant. As previously mentioned, in the United States alone, nearly 37,000 fatalities are attributed to motor vehicle crash last year. [12] To put this number in perspective, summing the traffic-related deaths over the last 30 years alone, is the equivalent to approximately all American war deaths in the 235 years of the country's existence. Such statistics are no longer germane to North America and Western Europe as sharp economic growth in developing countries has caused the social and economic toll of MVC to become an issue of global concern. The World Health Organization estimated that in 2004, 1.2 million deaths and nearly 20 million injuries were attributed to MVC, accounting for 2.2% of all deaths and costing between 1 and 2% of GDP in some nations. While computational modeling cannot solve this issue alone, these tools have the ability to put advanced injury assessment capabilities in the hands of engineers who design vehicular safety systems.

Simulated safety research has tremendous cost savings advantages over traditional physical vehicle testing as well. There is relatively little overhead in running simulations, whereas full-scale vehicle tests can run into the hundreds of thousands of dollars, and require large testing facilities. Traditional crash test dummies are also limited in their injury assessment capabilities. But, with a validated full-body model, where developers can program ribs to break at known strain values, or for lungs to be contused at known strain rates, this type of prediction becomes possible.

Conclusions

We have presented the design and development of a novel set of CAD data that describes the mid-sized male in the seated position. The CAD data represents 408 structures of the human body. The model was developed for subsequent use in FEA models aimed at predicting a set of specific and commonly encountered traumatic injuries. The CAD model was developed from a single individual that was scanned in multiple image modalities and postures. The M50 CAD data was derived from a carefully selected average male subject, and to that end, the morphologic data contained in this work can be used as an average male reference.

References

1. Yang, K.H., et al., *Development of numerical models for injury biomechanics research: a review of 50 years of publications in the Stapp Car Crash Conference.* Stapp Car Crash J, 2006. **50**: p. 429-90.
2. Gordon, C., et al., *1988 Anthropometric Survey of U.S. Army Personnel: Methods and Summary Statistics*, D.a.E.C. Prepared for United States Army Natick Research, Editor. 1989.
3. Schneider, L., et al., *Development of anthropometrically based design specifications for an advanced adult anthropometric dummy family, Vol 1.*, N. US Department of Transportation, Editor. 1983.
4. Cheng, H., L. Obergefell, and A. Rizer, *Generator of Body Data (GEBOD) , Manual.*, D.o.D. Air Force Material Command, Editor. 1994, Systems Research Labs Inc. p. 74.
5. Robbins, D., *Anthropometric specifications for mid-sized male dummy*, D.o. transportation, Editor. 1983, University of Michigan Transportation Research Institute. p. 134.
6. Spitzer, V., et al., *The Visible Human Male: A Technical Report.* JAMIA, 1996. **3**: p. 118-130.
7. Ruan, J., et al., *Prediction and analysis of human thoracic impact responses and injuries in cadaver impacts using a full human body finite element model.* Stapp Car Crash J, 2003. **47**: p. 299-321.
8. Ruan, J.S., et al., *Biomechanical Analysis of Human Abdominal Impact Responses and Injuries through Finite Element Simulations of a Full Human Body Model.* Stapp Car Crash J, 2005. **49**: p. 343-66.
9. Lee, J.B. and K.H. Yang, *Development of a finite element model of the human abdomen.* Stapp Car Crash J, 2001. **45**: p. 79-100.
10. Robin, S., *Human Model for Safety – A joint effort towards the development of redefined human-like car-occupant models.*, in *17th International Conference for the Enhanced Safety of Vehicles*. 2001: Amsterdam.
11. Seki, S. and H. Iwamoto, *Disruptive forces for swine heart, liver, and spleen: their breaking stresses.* J Trauma, 1998. **45**(6): p. 1079-83.
12. NHTSA, *Traffic Safety Facts 2008; A compilation of motor vehicle crash data from the fatality analysis reporting system and the general estimates system*, D.o. Transportation, Editor. 2008, National Highway Traffic Safety Administration.
13. Gayzik, F., et al., *Multi-Modality Image Data Collection Protocol for Full Body Finite Element Model Development*, in *SAE Digital Human Modeling*. 2009, SAE: Gothenburg, Sweden.
14. Mertz, H., *Anthropomorphic Test Devices*, in *Accidental Injury, Biomechanics and Prevention*, A. Nahum and J. Melvin, Editors. 1993, Springer-Verlag: New York.
15. Flannagan, C., et al., *An Improved Seating Accommodation Model with Application to Different User Populations*, in *SAE International Conference and Exposition*. 1998: Detroit, MI.
16. Manary, M., et al., *Human Subject Testing in Support of ASPECT*, in *SAE International Congress and Exposition*. 1999: Detroit, MI.
17. Reed, M.P., M.A. Manary, and L.W. Schneider, *Methods for Measuring and Representing Automobile Occupant Posture*, in *SAE International Congress and Exposition*. 1999: Detroit, MI.
18. Au, A.G., et al., *A NURBS-based technique for subject-specific construction of knee bone geometry.* Comput Methods Programs Biomed, 2008. **92**(1): p. 20-34.
19. Scherf, H. and R. Tilgner, *A new high-resolution computed tomography (CT) segmentation method for trabecular bone architectural analysis.* Am J Phys Anthropol, 2009.

20. Newman, D.L., et al., *Limitations of clinical CT in assessing cortical thickness and density.* Phys Med Biol, 1998. **43**(3): p. 619-26.
21. Prevrhal, S., K. Engelke, and W.A. Kalender, *Accuracy limits for the determination of cortical width and density: the influence of object size and CT imaging parameters.* Phys Med Biol, 1999. **44**(3): p. 751-64.
22. Dougherty, G. and D. Newman, *Measurement of thickness and density of thin structures by computed tomography: a simulation study.* Med Phys, 1999. **26**(7): p. 1341-8.
23. Gray, H., *Anatomy of the Human Body*. 20 ed, ed. L. Warren. 1918: Lea & Febiger. 1396.